Characterization of the $\Delta\mu_{H^+}$-Sensitive Ubisemiquinone Species (SQ_{Nf}) and the Interaction with Cluster N2: New Insight into the Energy-Coupled Electron Transfer in Complex I†

Takahiro Yano,*,§ William R. Dunham,‡ and Tomoko Ohnishi*,§

Johnson Research Foundation, Department of Biochemistry and Biophysics, School of Medicine, University of Pennsylvania, Philadelphia, Pennsylvania 19104, and Division of Plastic and Reconstructive Surgery, Department of Surgery, University of Michigan Medical School, Ann Arbor, Michigan 48109

Received August 30, 2004; Revised Manuscript Received October 22, 2004

ABSTRACT: In this report, we describe the electron paramagnetic resonance (EPR) spectroscopic characterizations of the fast-relaxing ubisemiquinone (SQ_{Nf}) species associated with NADH−ubiquinone oxidoreductase (complex I) detected in tightly coupled submitochondrial particles (SMP). The signals of SQ_{Nf} are observed only in the presence of $\Delta\mu_{H^+}$, whereas other slowly relaxing SQ species, SQ_{Ns} and SQ_{Nx}, are not sensitive to $\Delta\mu_{H^+}$. In this study, we resolved the EPR spectrum of the $\Delta\mu_{H^+}$-sensitive SQ_{Nf}, which was trapped during the steady-state NADH−Q_1 oxidoreductase reaction, as the difference between coupled and uncoupled SMP. Thorough analyses of the temperature profile of the resolved SQ_{Nf} signals have revealed previously unrecognized spectra from $\Delta\mu_{H^+}$-sensitive SQ_{Nf} species. This newly detected SQ_{Nf} signals are observable only below 25 K, similar to the cluster N2 signals, and exhibit a doublet signal with a peak-to-peak separation (ΔB) of 56 G. In this work, we identify the partner to the interacting cluster N2. We have analyzed the $g = 2.00$ and $g = 2.05$ splittings using a computer simulation program that includes both exchange and dipolar interactions as well as the g-strain effect. Computer simulation of these interaction spectra showed that cluster N2 and fast-relaxing SQ_{Nf} species undergo a spin−spin interaction, which contains both exchange (55 MHz) and dipolar interaction (16 MHz) with an estimated center-to-center distance of 12 Å. This finding delineates an important functional role for this coupled [$(N2)_{red}$−SQ_{Nf}] structure in complex I, which is discussed in connection with electron transfer and energy coupling.

NADH−ubiquinone oxidoreductase, complex I,[1] catalyzes electron transfer from NADH to ubiquinone-10 via a series of intrinsic redox centers and actively translocates protons across the mitochondrial inner membrane to generate electrochemical proton gradient $\Delta\mu_{H^+}$ (*1*−*4*). Complex I from bovine heart mitochondria is composed of at least 46 dissimilar subunits (*5*). Low-resolution electron microscopic images depict an asymmetric L-shaped form composed of two major parts: a membrane part embedded in a lipid bilayer and a hydrophilic peripheral part protruding into the matrix or cytoplasmic space (*6*−*11*). Complex I contains one noncovalently bound FMN (*12*) and eight iron−sulfur clusters (designated N1a and N1b for [2Fe−2S] centers and N2, N3, N4, N5, N6a, and N6b for [4Fe−4S] centers) to carry out the intramolecular electron transfer (*3*, *13*, *14*). The subunit locations of the FMN and all eight iron−sulfur clusters have tentatively been identified (*13*, *15*−*20*). The iron−sulfur cluster N2 has attracted the attention of investigators in the complex I field because of its pH dependence (−60 mV/pH) and highest apparent E_m value (*21*). This specific iron−sulfur cluster is thought to donate electrons directly to ubiquinone. Although the subunit location of cluster N2 has been under debate, recent site-directed mutagenesis studies with *Escherichia coli* (*20*) and *Yarrowia lipolytica* systems (*22*) have provided experimental data strongly supporting that cluster N2 is located in the PSST/NuoB subunit. All of the cofactor-binding subunits are located in the peripheral part (*5*). This indicates that the electron transfer from NADH through the iron−sulfur clusters occurs in the peripheral part, whereas the H^+ translocation takes place through H^+ transport pathways formed within the membrane part. These distinct functions of the two spatially separated parts of complex I must be mechanistically linked to each other to conserve energy (*2*, *4*).

Two very important and unanswered questions are the following: how is the H^+ translocation in the membrane part

† This work was supported by United States Public Health Service Grant No. R01GM30736 to T. Ohnishi.

* To whom correspondence should be addressed. For T.O., phone (215) 898-8024, fax (215) 573-3748, e-mail ohnishi@mail.med.upenn.edu; for T.Y., phone (215) 898-2939, fax (215) 573-3748, e-mail yano@mail.med.upenn.edu.

§ University of Pennsylvania.

‡ University of Michigan Medical School.

[1] Abbreviations: complex I, NADH−ubiquinone oxidoreductase; SMP, submitochondrial particles; Q_1, ubiquinone-1; SQ, ubisemiquinone; SQ_{Nf}, complex I associated fast-relaxing ubisemiquinone; SQ_{Ns}, complex I associated slowly relaxing ubisemiquinone; SQ_{Nx}, complex I associated very slowly relaxing ubisemiquinone; $\Delta\mu_{H^+}$, electrochemical proton gradient; E_m, midpoint redox potential; EPR, electron paramagnetic resonance; CCCP, carbonyl cyanide *m*-chlorophenyl hydrazon; EIPA, 5-(*N*-ethyl-*N*-isopropyl)-amiloride; FMN, flavin mononucleotide.

10.1021/bi048132i CCC: $30.25
Published on Web 01/14/2005

linked to the redox reaction, and what is the driving mechanism of the H^+ pump in the membrane? Complex I contains three potential subunits, which form the H^+ transport pathway, namely, ND2, ND4, and ND5, in the membrane part. These subunits are related via evolution to Na^+/H^+ antiporters in some bacteria (*23*−*25*). The ND1 subunit is a highly conserved subunit; however, the functional role of this subunit is still not fully understood (*26*−*28*). Only limited information is available to understand the structure and function of the membrane part of complex I. The ND5 subunit of bovine heart complex I has been labeled by a fenpyroximate photoaffinity analogue, which is correlated with inhibition of the enzyme activity and is prevented by EIPA, an inhibitor of Na^+/H^+ antiporters (*29*, *30*). The site-directed mutagenesis study of the ND2 subunit homologue of *E. coli* complex I has suggested that the subunit contains a Q-binding site (*31*). More recently, the ND4 subunit homologue of *E. coli* complex I was directly photoaffinity labeled by an azido-Q analogue (*32*). These experimental data suggest that the H^+ translocation in the membrane part is linked to the redox reactions mediated by Q. Possible Q-binding sites in ND4 and ND5 subunits have been proposed based on the amino acid sequence comparisons (*33*). Therefore, it is probable that the oxidation and reduction of Q can be an integral component of the driving mechanism of the H^+ pump and that the interface between the hydrophilic and hydrophobic parts most likely holds a key to elucidate the coupling mechanism, where a crucial component, cluster N2, is located as a direct electron donor to Q species. However, the electron-transfer steps involving cluster N2 and ubiquinone has remained unknown.

Vinogradov et al. reported that ubisemiquinone (SQ) signals are detectable in the complex I segment of the mitochondrial respiratory chain during steady-state oxidation of NADH or succinate (*34*−*36*; also see citations in these refs) (expressed hereafter as NADH → O_2 and succinate → O_2 reaction). Physicochemical properties of these SQ species differ considerably, specifically in their spin relaxation behavior, allowing us to distinguish them as SQ_{Nf} (fast), SQ_{Ns} (slow), and SQ_{Nx} (very slow) species (*34*, *35*). The SQ_{Nf} signals are observed only in the presence of $\Delta\mu_{H^+}$, whereas both SQ_{Ns} and SQ_{Nx} species are insensitive to $\Delta\mu_{H^+}$ (*34*−*37*). Because semiquinones have their spin densities distributed over several atoms, their spin relaxation rates are most strongly determined by the presence of nearby spin systems via spin−spin interactions. The markedly different properties of the SQ species, therefore, indicate that these SQ species are located at different sites in the enzyme complex and may play distinct roles (*38*) or that their neighboring redox centers are in differing redox states indicating a different location in the electron pathway. Hence, to better understand the electron-transfer coupled to H^+ translocation of complex I, it is important to individually characterize these SQ species in more detail. We are particularly interested in the SQ_{Nf} species, because this SQ species is extremely sensitive to $\Delta\mu_{H^+}$ posed across the mitochondrial inner membrane. The highly enhanced spin relaxation of the SQ_{Nf} is an indication of the spin coupling with tetranuclear iron−sulfur clusters (*36*, *38*). We have proposed mutual interaction between the SQ_{Nf} and cluster N2 based on a close correlation between a line shape alteration of the $g_z = 2.05$ signal (either splitting or broadening) of cluster N2 and quenching of the SQ_{Nf} signal under various conditions (*34*). The 33 G splitting of the $g_z = 2.05$ signal of cluster N2 has been confirmed by two different groups; however, solid experimental evidence to identify the partner of the spin coupling with cluster N2 has not yet been obtained. In the NADH → O_2 or succinate → O_2 systems, significant overlaps of free radical signals from SQ species formed within complex II and III make further analysis very difficult. Particularly, since the $\Delta\mu_{H^+}$-sensitive SQ_{Nf} species is so far detectable only in the steady-state reaction in the coupled SMP, it is essential to establish experimental conditions to resolve them spectroscopically and characterize different SQ species. We have limited the enzyme reaction in the complex I segment by using an exogenous electron acceptor, ubiquinone-1, in the presence of inhibitors of complexes II and III. Some of the preliminary data have been reported earlier (*34*, *38*).

In the present study, we report more detailed characterization of physicochemical properties of the $\Delta\mu_{H^+}$-sensitive SQ_{Nf} species in the steady-state NADH → Q_1 reaction. We discovered that while the SQ_{Nf} species exhibits a usual isotropic EPR line shape at high temperature, below 25 K the SQ_{Nf} species shows 56 G splitting centered at the $g = 2.004$ SQ signal, which has not been recognized previously. We analyzed this new spin−spin interaction signal with a computer simulation program that includes both exchange and dipolar interactions as well as *g*-strain effects (*39*, *40*). Both 33 and 56 G splitting of cluster N2 and SQ_{Nf} spectra, respectively, were fit with the same exchange (55 MHz) and dipolar (16 MHz) coupling parameters with a center-to-center distance of 12 Å, indicating that the interaction between these two redox centers does in fact cause the splitting of the respective EPR lines. These new findings shed light on the dynamic electron-transfer reactions in the catalytic core region of complex I, which is tightly coupled to the H^+ translocation.

EXPERIMENTAL PROCEDURES

Preparation of Mitochondria and Submitochondrial Particles. Bovine heart mitochondria and submitochondrial particles (SMP) were prepared according to the methods previously described (*41*). The SMP was then treated with appropriate amounts of oligomycin to block proton leak through ATP synthase, thereby increasing the efficiency of energy coupling in SMP (*42*). Complex I was activated by the method of Kotlyar and Vinogradov (*41*). To study effects of pH, the activated SMP was centrifuged and suspended in different pH buffer containing 50 mM each of MOPS, Tris, or HEPES. The pH of the buffers was adjusted by HCl or NaOH to desired values. The suspensions were ultracentrifuged again and suspended in the buffers. The pH of the final SMP suspensions was directly checked by a pH meter. For H_2O/D_2O exchange experiments, the final suspension buffer was prepared with 99% D_2O (Sigma), and pH instead of pD was adjusted with HCl and a pH meter. The activated SMP was ultracentrifuged at 167 000 × *g* for 20 min, and the pellets were suspended in D_2O buffer. This process was repeated at least three times to exchange H_2O with D_2O.

For the standard activity assay, SMPs (50−100 μg of protein/mL) were preincubated in a standard reaction mixture containing 0.25 M sucrose, 50 mM Tris-HCl (pH 8.0), 0.2 mM EDTA, and 1 mg/mL bovine serum albumin. The

reaction was initiated by adding 100 μM NADH (at the final concentration) and the decrease of absorbance at 340 nm was monitored by spectrophotometer. For uncoupling, CCCP was added to be 27 μM.

EPR Sample Preparation. EPR samples were prepared as follows. The activated SMPs were suspended in the reaction buffer to be 25 mg/mL. The suspension in a glass test tube was kept on ice with a constant stirring with a small magnet bar. Antimycin, myxothiazol, carboxin, and Q_1 (decyl-UQ, nonyl-UQ) were subsequently added slowly, and the mixtures were incubated on ice for at least 1 h. The suspension was split into two equal portions, and CCCP was added into one-half for an uncoupled sample. These treated SMPs were transferred into EPR tubes, and the tubes were preincubated at 25 °C for 1 min. The NADH-Q_1 oxidoreductase reaction was initiated by adding NADH using a specially designed rapid mixing device. The mixtures were rapidly frozen in dry ice/ethanol mix, typically within 5−7 s after adding the substrate, and the EPR sample tubes were stored in liquid nitrogen until analysis.

EPR Measurements. EPR spectra were recorded by a Bruker ESP 300E spectrometer at X-band (9.4 GHz) with an Oxford Instrument ESR900 helium flow cryostat, a Hewlett-Packard microwave frequency counter 5350B and a temperature controller ITC4 to control sample temperatures. EPR conditions are described in legends to figures in detail.

Computer Simulations. The computer program used in these simulations was written by K. Schepler originally for use on samples from another part of the respiratory chain (*43*, *44*). It is a second-order perturbation theory calculation of a spin−spin interaction between two $S = {}^1/_2$ spin systems, interacting via the dipole−dipole and the exchange coupling, where the size of this interaction is small compared to the size of the Zeeman splitting of the interacting spins but otherwise unconstrained. Since its original form, the program has been rewritten to include the complexity of "*g*-strain" (*45*−*47*) in the interacting spins and to include automatic spectral fitting using a form of principal-axis minimization with quadratic interpolation (*48*).

The complete Hamiltonian is given by

$$\mathcal{H} = \beta\vec{H}\cdot\tilde{G}_1\cdot\vec{S}_1 + \beta\vec{H}\cdot\tilde{G}_2\cdot\vec{S}_2 - 2J\vec{S}_1\cdot\vec{S}_2 + \frac{\vec{\mu}_1\cdot\vec{\mu}_2}{r^3} - \frac{3(\vec{\mu}_1\cdot\vec{r})(\vec{\mu}_2\cdot\vec{r})}{r^5}$$

where the first two terms are the electron Zeeman terms, which account for the EPR spectra of isolated spin systems. The next term is the exchange interaction, shown here as a scalar interaction because of its small size relative to the electron Zeeman terms and the magnetic dipole−dipole interaction. The last two terms are the dipolar term, which is also assumed to be small relative to the Zeeman terms but not small relative to the exchange terms. With these assumptions, the Hamiltonian can be set up in a frame in which the Zeeman terms are on the diagonal of the Hamiltonian matrix. This frame is commonly referred to as the prime frame by Abragam and Bleaney (*49*) and is the frame of which the *z*-axis is parallel to the *z*-axis of the quantization system. Thus, the Zeeman terms are written as some constants times the operators S'_{1z} and S'_{2z}. This frame is also one in which the exchange and dipolar terms are concentrated into four elements of the 4 × 4 Hamiltonian matrix. Because the Hamiltonian has this block diagonal form it can be "diagonalized" algebraically by solving a quadratic equation. With the solution of the energy Hamiltonian, the wave functions rotated back to lab frame to calculate the transition intensities. This process is repeated for each "crystal-frame" orientation to form the powder spectra shown in Results. There are small terms off the diagonal, which can be ignored in the present spectra but can be important to the so-called "half-field" resonances, especially their intensities. These are calculated with conventional second-order perturbation theory but are irrelevant to this study, because we observed no half-field resonances. A complete parameter set for the relevant spectra includes three *g*-values and three line widths for each of the interacting centers, plus the four parameters that describe the interaction, the magnitudes of *J* (exchange coupling constant) and *r* (center-to-center distance) and polar angle (ψ) and azimuthal angle (η), necessary to specify the direction of the **r**-vector in the crystal frame as shown in Scheme 1. We assumed that the N2 *g*-values are nearly equal in the G_{xy} regions, but the spectra are independent of their exact values. We assumed that the *g*-values and line widths are isotropic for the semiquinone. All of these parameters are described in Results. The theory and the spectra are independent of the sign of *J*. There is no *D* because the dipole interaction is given by

Scheme 1

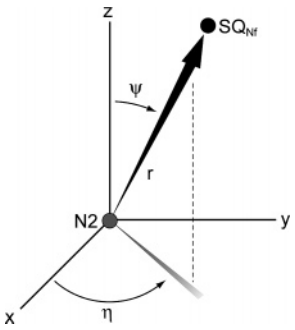

$$\mathcal{H} = \frac{\vec{\mu}_1\cdot\vec{\mu}_2}{r^3} - \frac{3(\vec{\mu}_1\cdot\vec{r})(\vec{\mu}_2\cdot\vec{r})}{r^5}$$

This is the interaction that is calculated to 2nd-order, not the expansion of its operator equivalent. This complexity is well-described by the quoted papers by Schepler et al. (*43*, *44*). We chose this method because we found that by using the above-mentioned method of calculation we were able to construct an exact representation of the classical dipole operator without recourse to an expansion in the Hilbert space. This method of calculation is not available if the exchange term is large as it is for the work of Stevenson et al. (*40*) from our laboratory. Here, the off-diagonal terms in the *J*-matrix and their representation in the Hilbert space must be included. However, it is interesting to note that even in this space the matrix can be diagonalized algebraically, albeit not easily because the secular equation is cubic.

Reagents. All chemicals were of the highest grade available from Sigma-Aldrich.

RESULTS

To optimize our experimental condition, we examined the effects of pH on the NADH-Q_1 oxidoreductase activity in

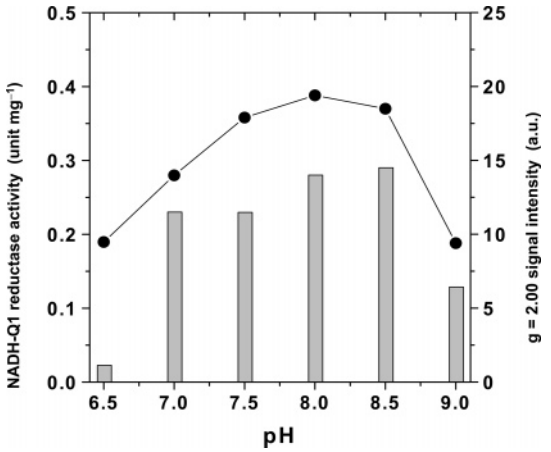

FIGURE 1: The effects of pH of the NADH−Q_1 oxidoreductase activity of submitochondrial particles (SMP) in the absence of CCCP and on the EPR signal of the $\Delta\mu_{H^+}$-sensitive SQ_{Nf} species. The NADH−Q_1 oxidoreductase activity (●) was measured as described in Experimental Procedures. The EPR spectra of the coupled and uncoupled samples were measured at 40 K at 20 mW. The $\Delta\mu_{H^+}$-sensitive SQ_{Nf} EPR spectra were resolved as difference spectra. The signal amplitude of the SQ_{Nf} signals (peak-to-peak) was measured. EPR conditions are microwave frequency = 9.422 GHz, modulation frequency = 100 kHz, modulation amplitude = 5.085 G, conversion time = 81.9 ms, and time constant = 163.8 ms.

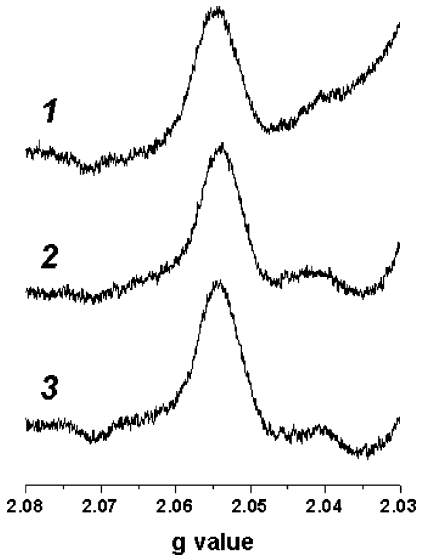

FIGURE 2: EPR spectra of $g = 2.05$ region of SMP. The SMP samples (pH 8.5) were prepared as described in Experimental Procedures. Spectrum 1 shows coupled SMP; spectrum 2 shows uncoupled SMP; spectrum 3 shows fully reduced SMP. EPR signals were an average of four scans. EPR spectra were measured at 16 K and 10 mW. Other EPR conditions are the same as those in Figure 1 except for microwave frequency = 9.421 GHz.

SMP used in this study. As we previously reported (*38*), the NADH-Q_1 oxidoreductase (NADH → Q_1) activity had its optimal pH only in a narrow range between 7.5 and 8.5. At pH 8.0, the electron-transfer rates were 0.56 and 0.38 μmol of NADH oxidized per minute per milligram of protein in the presence and absence of CCCP, respectively (Figure 1). Both reactions were inhibited more than 90% by 1 μM rotenone. At pH 6.0 and pH 9.0, the activities decreased to ~0.27 and ~0.19 μmol of NADH oxidized per minute per milligram of protein in the presence and absence of CCCP, respectively. A respiratory control ratio (RCR) was 1.2−1.5 within this pH range. RCR of the same SMP was determined to be ~7 for the NADH oxidase reaction (NADH → O_2); in the presence of CCCP; the activity was 1.5 μmol of NADH oxidized per minute per milligram of protein, indicating that the SMP preparations used were tightly coupled (*38*). The low RCR value for NADH−Q_1 oxidoreductase was caused by a low membrane proton motive force generated by the NADH−Q_1 oxidoreductase (NADH → Q_1) as compared to those by NADH−O_2 (NADH → O_2) and succinate−O_2 (succinate → O_2) reactions. Despite the low RCR value in the complex I segment (NADH → Q_1) of the respiratory chain, we clearly discerned distinct redox and spectral behaviors of SQ species in coupled and uncoupled SMP, as shown below.

Redox State of Cluster N2 in the Steady-State NADH → Q_1 Reaction. In the steady-state NADH → Q_1 reaction, we examined the redox state of iron−sulfur clusters of complex I, especially, cluster N2, a key redox component in the Q reduction processes. Cluster N2 has the highest apparent midpoint redox potential ($E_{m,7}$ = −150 to −50 mV) in complex I of bovine heart SMP. The E_m value of cluster N2 is variable dependent on complex I preparations. The reduction state of N2 during turnover can, therefore, be indicative of whether the reactions involving N2 are rate-limiting or not. In the steady-state NADH → O_2 reaction, cluster N2 is almost fully reduced, whereas clusters N3 and N4 are partially reduced to 50−70% (*34*, *50*). At 16−18 K with microwave power levels of 1−10 mW, the $g_z = 2.05$ EPR signal of cluster N2 is readily detectable without overlapping signals from other tetranuclear iron−sulfur clusters in complex I (*34*). When the $g_z = 2.05$ signals were compared among the coupled, uncoupled, and "fully reduced SMP" samples at 16 K and 10 mW, the reduction levels of cluster N2 in the coupled and uncoupled SMP were found to be the same as that of the "fully reduced SMP" (Figure 2). Clusters N3 and N4 were only partially reduced in the coupled and uncoupled samples, and their reduction levels were almost the same under these two conditions. These observations indicate that the intramolecular electron transfer through the iron−sulfur clusters of complex I in SMP resembles that in the steady-state NADH → O_2 reaction. The electron transfer from flavin to cluster N2 is not the rate-limiting step in either coupled or uncoupled states in the steady-state NADH → Q_1 reaction.

EPR Characterization of the Resolved SQ_{Nf} Species. Figure 3A shows EPR spectra at the $g = 2.00$ region of the SMP samples in the steady-state NADH → Q_1 reaction in the absence and presence of uncoupler CCCP (pH 8.5) measured at 40 K. The difference spectrum gave an isotropic SQ EPR spectrum with a central transition at $g_{z,y,x} = 2.004$. The amplitude of the SQ free radical signal is much smaller than that observed in the steady-state NADH → O_2 reaction. This is partly due to the elimination of SQ signals arising from other respiratory complexes. This is also caused by a lower enzyme turnover and lower $\Delta\mu_{H^+}$ generated in this system. Nevertheless, the $\Delta\mu_{H^+}$-sensitive SQ component is evident by comparing the spectra in the absence (spectrum 1) and presence (spectrum 2) of CCCP. As reported earlier (*34*), the power saturation analysis revealed the presence of both fast-relaxing SQ_{Nf} species and slowly relaxing SQ_{Ns} species in the $g = 2.004$ signals from coupled SMP. In contrast, only slowly relaxing SQ_{Ns} species is seen in uncoupled SMP

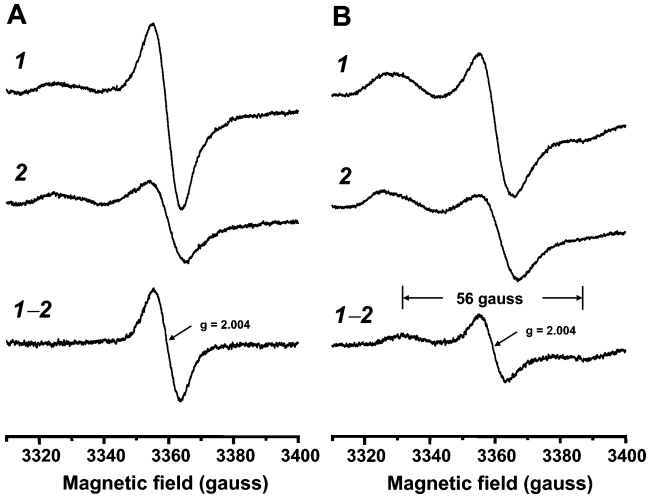

FIGURE 3: EPR spectra of $g = 2.00$ region of the coupled and uncoupled SMP and the difference spectra [coupled] − [uncoupled]: (A) EPR spectra of $g = 2.00$ region measured at 40 K and 1 mW; (B) EPR spectra of $g = 2.00$ region measured at 20 K and 1 mW; (1) coupled SMP; (2) uncoupled SMP; (1 − 2) difference spectrum [coupled] − [uncoupled]. EPR conditions are the same as Figure 1 except that microwave frequency was 9.423 GHz and EPR spectra are an average of nine scans.

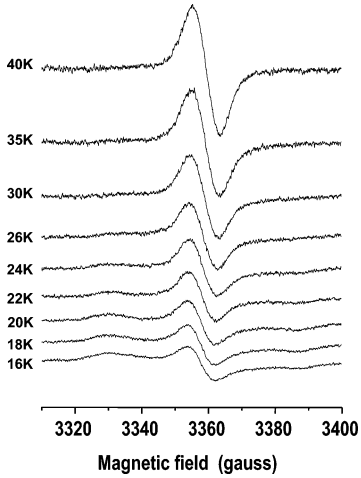

FIGURE 4: Temperature dependence of the resolved EPR spectra of the $\Delta\mu_{H^+}$-sensitive SQ_{Nf} species detected in the steady-state NADH−Q_1 oxidoreductase reaction at pH 8.5. EPR spectra were measured at different sample temperatures (16−40 K). The EPR spectra have been corrected for the temperature effects from the Curie law. Other EPR conditions are same as those in Figure 3.

(data not shown). The EPR spectra of the $\Delta\mu_{H^+}$-insensitive SQ components in both coupled and uncoupled samples were almost identical (*34*). Therefore, the $\Delta\mu_{H^+}$-sensitive SQ species can be spectroscopically resolved by taking a difference spectrum between coupled and uncoupled SMP in the steady-state NADH → Q_1 reaction (spectrum 1 minus spectrum 2). This difference spectrum should represent the spectrum of the "fast SQ" because it has characteristically very short spin relaxation times. These difference spectra allowed us to investigate EPR properties of the $\Delta\mu_{H^+}$-sensitive SQ_{Nf} species in detail. We also used decyl-UQ or nonyl-UQ as an exogenous substrate at pH 8.0 (*51*). The same results were obtained with both substrates (data not shown).

We analyzed the temperature profile of the $\Delta\mu_{H^+}$-sensitive SQ_{Nf} spectra between 16 and 100 K. It was found that the resolved SQ_{Nf} signal dramatically changes line shape below 40 K as shown in Figure 4.

Temperature Dependence of the SQ_{Nf} Signal in the Lower Temperature Range. Within a higher temperature range (25−100 K), the EPR spectra of the SQ_{Nf} showed a characteristic isotropic EPR line shape with $g_{z,y,x} = 2.004$ and $\sigma = 0.0030$ (line width expressed in *g*-units) as a single component of Gaussian line shape. Figure 4 shows the stacked difference spectra at various temperatures (16−40 K) with the intensity corrected for the temperature effect from the Curie law. The signal intensity of this species is almost constant over the temperature range from 40 to 35 K. Relatively minor broadening of the central free radical EPR line shape was observed by lowering temperature. A peak-to-peak line width of the $g = 2.004$ signal is $\Delta H_{pp} = 7.7$ G at 60 K and higher. At lower temperatures, the line width became slightly broader: $\Delta H_{pp} = 8.4$ G at 40 K and $\Delta H_{pp} = \sim 8.8$ G at 25 K. The signal intensity increased as the temperature decreased to below 25 K concomitant with the appearance of the 56 G doublet. Figure 3B presents EPR spectra of coupled (spectrum 1) and uncoupled (spectrum 2) SMP trapped in the steady-state NADH → Q_1 reaction in the presence of complexes II and III inhibitors recorded at 20 K and 1 mW. The difference spectrum (spectrum 1 minus spectrum 2) clearly exhibited a doublet signal with $\Delta B = 56$ G with $g_{z,y,x} = 2.004$ signal in the center. The amplitude of the doublet signals increased as temperature was lowered to 20 K and became roughly constant within the temperature range of 16−20 K, whereas the signal intensity of the nonsplit $g = 2.00$ signal decreased by a factor of more than three over this temperature range (Figure 4). When the temperature was lowered below 16 K, EPR signals arising from iron−sulfur clusters (S3 of complex II) became stronger, interfering with the split signal at the $g = 2.01-2.02$ region (data not shown).

Both the line width narrowing of the isotropic SQ free radical signal and the disappearance of the doublet signals with increasing temperature were due to the effects of thermal averaging of a nearby iron−sulfur cluster. The EPR line width (due to lifetime of an iron−sulfur cluster) is extremely temperature-sensitive as a result of the high-spin iron ions that comprise these centers.

pH Dependence and Effects of H_2O/D_2O Exchange on the SQ_{Nf} EPR Signal. We examined effects of buffer pH on the resolved SQ_{Nf} spectrum at 40 K. As briefly reported earlier (*38*), the SQ_{Nf} EPR signal showed unique pH dependence. The signals were clearly observed within a pH range between pH 7.0 and pH 8.5 but diminished abruptly below pH 6.5 and above pH 9.0. Because of the narrow peak-to-peak line width of <9 G, this SQ species is considered to be anionic within this pH range. The effects of pH on the low-temperature SQ_{Nf} EPR signal, however, differ from those on the $\Delta\mu_{H^+}$-insensitive SQ_{Ns} anion. In the uncoupled SMP, the EPR signal arising from the SQ_{Ns} steadily increases with pH, as expected for the usual SQ anion (*38*). The pH profile of the SQ_{Nf} EPR signal did not follow the pH profile of the general SQ anion but was parallel to the pH dependence of NADH−Q_1 oxidoreductase activity in the absence of CCCP as shown above (Figure 1). Since the SMPs used in this study were tightly coupled, it is concluded that the $\Delta\mu_{H^+}$ generated by the redox-coupled reactions stabilizes the SQ_{Nf} species.

To further examine the protonation state of the SQ_{Nf} species, we exchanged H_2O with D_2O to examine isotope

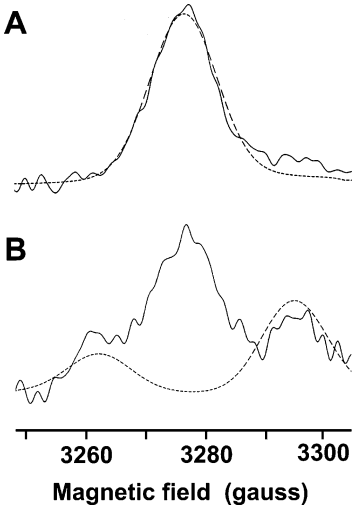

FIGURE 5: EPR spectra of the $g_z = 2.05$ signal of cluster N2 detected in the fully reduced SMP (A) and in the tightly coupled SMP in the steady-state succinate → O_2 reaction (B) and computer simulated spectra. These EPR spectra were reproduced from Figure 6 in ref *34*. The EPR spectra were measured at 16 K and 1 mW for spectrum A and 18 K and 10 mW for spectrum B. EPR conditions were the same as those in Figure 1 except for microwave frequency of 9.422 GHz. The individual experimental EPR spectra were simulated (broken lines) as described in Experimental Procedures.

effects on an EPR line shape of the SQ_{Nf} signal. If the SQ species is in a protonated form ($QH^{\bullet}$), H_2O/D_2O exchange should affect the line width of the signal. No difference was observed in line width and line shape, confirming that the SQ_{Nf} species is in an anionic form ($Q_{Nf}^{\bullet -}$), as indicated by the narrow $\Delta H_{pp} < 9$ G in comparison with the $\Delta H_{pp} = 10-12$ G for the $QH^{\bullet}$ (Figure 4).

Computer Simulation of the Split EPR Signals of SQ_{Nf} and Cluster N2. From the result of Figure 4, let us hypothesize that the spin−spin interaction between cluster N2 and the SQ_{Nf} is discernible below 25 K. Then, known parameters for these two interacting centers are their g values and line widths: $g_z = g_y = g_x = 2.0043$ and $\sigma_{z,y,x} = 0.0030$ (g-units) for SQ_{Nf}, and $g_z = 2.05$, $g_x = g_y = 1.92$ for cluster N2. The axial g values are not very important in this calculation because only the interaction along the g_z-axis of the iron−sulfur cluster is visible in the relevant spectrum. Using $g_z = 2.054$ and a line width of 0.0048 (g-units), we achieved the fit as shown in Figure 5A. As described in the computer simulation part of the Experimental Procedures, there are four parameters left to describe this quantum system if we ignore g-strain. Three of these parameters describe the distance (distance is important to the dipole−dipole interaction) and direction of the dipole−dipole interaction. In the axis system describing the iron−sulfur **g**-tensor, ψ, η, and r describe the polar angle, the azimuthal angle, and the intercenter distance, respectively. The fourth parameter is J, the exchange coupling constant, given in MHz and defined by the following equation: $\mathscr{H} = -2\vec{J}\vec{S}_1 \cdot \vec{S}_2$. Thus, this computer program was found to be applicable for the problem of a SQ interacting with another spin system (cluster N2) in complex I. In this system, cluster N2 is about 50% reduced.

The effect of the dipole−dipole interaction depends on the orientation of the intermolecular vector, **R**, with respect to the applied magnetic field. The interaction is twice as strong when **R** is oriented along the applied field direction as compared to the perpendicular orientations. We achieved a computer fit with the following parameters: $r = 12$ Å, $\psi = 65°$, $\eta = 0°$, and $J = 55$ MHz. It should be emphasized that Figure 5B is an output from the same computer program and has the same simulation parameters as Figure 5A, but with the four additional spin−spin parameters. With this parameter set, we simulated the $g = 2.00$ signal. As shown in Figure 6, a good fit to the 56 G doublet was also attained using the same spin−spin simulation parameters used in Figure 5B.

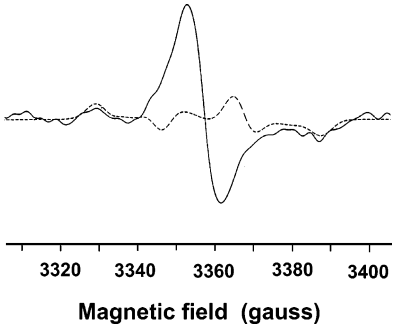

FIGURE 6: EPR spectrum of the SQ_{Nf} species measured at 16 K and 1 mW and computer simulated spectrum of the doublet SQ_{Nf} spectrum. The experimental EPR spectrum of the SQ_{Nf} was measured under the condition described in Figure 3. The spectrum was simulated (− − −) as described in Experimental Procedures.

The main goal of this fitting model is to show that it is possible to simulate simultaneously the $g = 2.05$ splitting (33 G) and $g = 2.00$ splitting (56 G) with the same interaction parameter set. We conclude that EPR spectra strongly indicate that cluster N2 and SQ_{Nf} are interacting in complex I at a center-to-center distance of 12 Å. Previously, EPR analysis of the multilayered oriented membrane preparation revealed that the g_z direction of cluster N2 corresponds to a unique angle, perpendicular to the membrane plane (*52*). Combining this information with the current computer simulation data, the N2−SQ_{Nf} vector angle is optimal at 65° ± 10° from the normal to the membrane, which is much closer to the in-plane direction.

$g_z = 2.05$ Signal Splitting in the NADH−Q_1 Oxidoreductase. We examined the effects of $\Delta\mu_{H^+}$ on the $g_z = 2.05$ EPR signals in the steady-state NADH → Q_1 reaction. We measured difference spectra, ([coupled] minus [uncoupled]), around the $g = 2.05$ region at 16 K and at different incident microwave power levels similar to the characterization of the SQ_{Nf} species described above. The spectra are shown in Figure 7. Although the signal amplitude was very small, we could observe some differences in the $g = 2.05$ region. At high power levels (5 and 10 mW), clear positive changes in signal amplitude were seen at 3295 and 3263 G with a peak separation of ∼33 G. The signal at 3295 G is higher than that at 3263 G. These two positive signals are similar to that of the computer simulation of the splitting signal of the $g_z = 2.05$ signal of cluster N2 shown in Figure 5B. The remaining small unsplit 2.05 signal is discerned in the center position of the split signals at the microwave power level of 10 mW (Figure 7).

DISCUSSION

Previously, it has been reported that cluster N2 displays interaction fine structure at $g_z = 2.05$ resonance in the

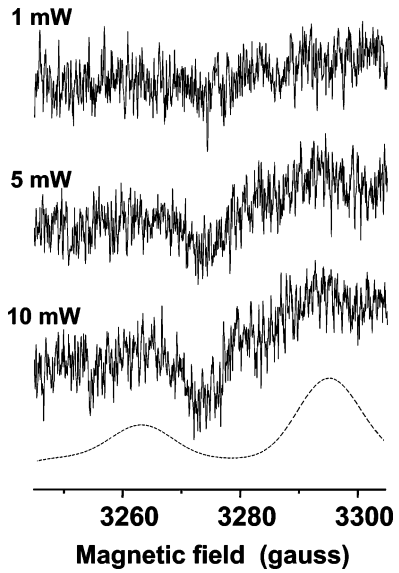

FIGURE 7: Difference spectra, [coupled] − [uncoupled], at $g = 2.05$ region. The EPR spectra of the coupled and uncoupled SMP in the steady state of NADH → Q_1 reaction were measured at 16 K at 1, 5, and 10 mW. EPR conditions are the same as those in Figure 3. The simulated spectrum of the split $g_z = 2.05$ EPR signals of cluster N2 is shown at the bottom for comparison.

coupled SMP in the steady-state reactions of NADH → O_2 or succinate → O_2. The g_z signal shows splitting with $\Delta B = 33$ G centered at $g_z = 2.05$. The previous EPR characterization of the split signals at multiple frequencies has demonstrated that the doublet signals result from a spin−spin interaction (*50*). Nevertheless, the cause of this splitting has not been found. While the spin−spin interaction between cluster N2 and the SQ_{Nf} has been proposed to show such splitting on cluster N2 EPR spectra (*34*, *35*, *53*), it has also been suggested that the $\Delta B = 33$ G (cf. 29 G) splitting is the result of the spin−spin interaction between two clusters N2 in the TYKY subunit, which is induced by protein conformational changes driven by the membrane proton motive force, $\Delta\mu_{H^+}$ (*50*). In the present study, we successfully detected the SQ_{Nf} EPR signals, which showed the splitting with $\Delta B = 56$ G at temperatures lower than 25 K. Therefore, it is possible that the doublet SQ_{Nf} EPR signal is the result of the spin−spin interaction with the paramagnetic cluster N2 spin system; however, we were puzzled by the fact that the observed splitting for the $g_z = 2.05$ signal was 33 G while the $g = 2.00$ splitting showed a doublet signal with a splitting almost twice as large of $\Delta B = 56$ G. This disparity in the size of the two splitting signals raises the question of whether the interaction signals observed in these two spin systems are related to each other because the same amplitude of splitting is generally expected to appear for two interacting paramagnetic centers when only dipole−dipole interaction is taken into account with *g*-value corrections. We decided to reinvestigate this issue using a computer simulation program that includes both exchange and dipole−dipole interactions to describe the interaction between two arbitrary **g**-tensor, *g*-strained spin systems. As we have reported before (*34*), 33 G splitting of the g_z signal of cluster N2 was most clearly detected in the tightly coupled SMPs during the steady state of the electron reverse from succinate to NAD^+, utilizing $\Delta\mu_{H^+}$ attained by succinate → O_2 reaction. Therefore, our present computer simulation data on the g_z splitting of cluster N2 are from that electron reverse system. The purpose of Figure 7 is to show that this splitting is also visible when the electron transfer is run in the forward direction, albeit with great difficulty.

Before discussing the observed EPR signals, it is necessary to emphasize some general properties of spin−spin interaction with a semiquinone. Because in a semiquinone, an $S = {}^1/_2$ electron spin resides in a π-system of the molecule, the spin−lattice relaxation time (EPR lifetime) is not readily affected by changes in the nearby atoms. This isolation is because the Zeeman interaction energy of the spin system is several orders-of-magnitude smaller than available phonon energies. Therefore, stable forms of magnetically isolated semiquinones (in flavodoxin, for example) are observable by EPR even at room temperature in liquid solution. On the other hand, $S = {}^1/_2$ forms of iron−sulfur clusters have lifetimes so short that they are only observable near liquid helium temperatures. In this case, the spin systems contain energy differences that are comparable to the phonon energies, thus encouraging energy transfer. Spin−spin interaction between these two $S = {}^1/_2$ spin systems is, therefore, likely to be observable only at very low temperatures when the iron−sulfur cluster is relaxing slowly and can display an EPR signal.

As the temperature is raised from 16 K, two phenomena are likely to be seen: (1) the EPR signal of the iron−sulfur cluster (and its interaction) will become smaller at temperatures between 30 and 150 K; (2) with increasing temperature, the faster spin relaxation rate of the iron−sulfur cluster will augment the spin relaxation of the semiquinone via a spin−spin interaction. In this case, even though the interaction between the spin systems is not visible in their EPR spectra, it can still result in a rapid relaxation of the semiquinone EPR signal.

As a consequence, there are some general properties of the EPR signals from these centers in conjugate proteins. For example, studying the line width of a SQ in a conjugate protein amounts to study the surrounding iron−sulfur clusters because they usually determine the line width of the SQ. It is difficult to estimate the effect of a spin−spin interaction on the line width of a SQ at high temperatures. Thermal averaging of spins in the interacting iron−sulfur cluster tends to narrow the SQ signal with increasing temperature. Increased relaxation of SQ spin system due to interaction with the thermally averaged iron−sulfur cluster tends to broaden the SQ signal via "lifetime broadening". Therefore, estimating the strength of the spin−spin interaction and the distance between interacting spins based on the SQ line width is not a simple matter.

Spin−Spin Interaction between Cluster N2 and the SQ_{Nf}. In this study, we have analyzed the interaction EPR spectra at $g = 2.00$ and at $g = 2.05$ and have achieved computer fits to these spectra with individual *g* values and line widths and four common additional parameters to describe this quantum system. A dominant exchange coupling (55 MHz) is present between these two redox centers, cluster N2 and SQ_{Nf}, in addition to the dipolar interaction (16 MHz), while their center-to-center distance is 12 Å. The formation of this transition intermediate structure [$(N2)_{red}$−SQ_{Nf}] explains the novel spin-relaxation properties of the SQ_{Nf} EPR signal as due to the spin relaxation properties of cluster N2. The exchange interaction (implying overlap of electron orbitals) resulted in the *g*-shift of cluster N2 EPR signal; the g_z =

2.054 for the noninteracting system becomes $g_z = 2.050$ in the interacting system. This shift indicates that there is a significant change in the geometry of cluster N2 (or its nearby environment) concomitant with the exchange interaction with SQ_{Nf}. This is another confirmatory correlation with the presence of the direct interaction between these two spin systems.

We have detected two SQ_{Nf} EPR signals, nonsplitting SQ and doublet SQ signals, in a different temperature range. A question remains as to whether these EPR signals arise from the same system. The short answer is that we have no information that they are not the same system. If cluster N2 and the SQ are exchange-coupled, then they could generate the doublet EPR spectrum shown in Figure 3B. As the temperature is increased, we would expect the EPR spectrum of the cluster N2 to broaden and disappear (as it does), the interaction spectrum of the SQ to disappear (as it does), and the spin relaxation time associated with SQ_{Nf} to increase (which it does). Furthermore, from Figure 4, it is clear that at least 70% of the nonsplitting SQ_{Nf} signal has become something else at low temperature. The obvious explanation is that this decreased nonsplitting SQ_{Nf} signal has become the doublet SQ_{Nf} signal by lowering the temperature.

A Role of the SQ_{Nf} Species in the Energy-Transducing Electron-Transfer Reactions. We defined the SQ_{Nf} species as an anion and found that its behaviors were considerably different from those of known anionic SQ species such as the $Q_s^{\bullet-}$ in complex II (*54*), the $Q_i^{\bullet-}$ in complex III (*55*), and the $Q_B^{\bullet-}$ in the bacterial reaction center (*56*). The latter three SQ species are thermodynamically stable and generally not sensitive to $\Delta\mu_{H^+}$. These SQ species are responsive to local pH and their stability constants are enhanced following a pH increase. These SQ species function as $n = 1 \leftrightarrow n = 2$ converters in the respective enzyme complexes, catalyzing the complete reduction of Q to QH_2. We have reported earlier that this type of SQ species is present in complex I, which is the $\Delta\mu_{H^+}$-insensitive SQ_{Ns} species (*38*, *77*). The SQ_{Ns} is an anion and thermodynamically stable. This species is located >30 Å away from the paramagnetic cluster N2 and thus distinct from the SQ_{Nf} species. The SQ_{Ns} is most likely bound to the site where a substrate Q is completely reduced to QH_2 (*38*). In the electron-transfer scheme from cluster N2 to the Q pool, we propose that the SQ_{Nf} species catalyzes the $n = 1$ electron transfer between Q and $Q^{\bullet-}$ as a bound form of Q and transfers electrons to the substrate Q binding site. In contrast to the SQ_{Ns}, the SQ_{Nf} EPR signal exhibited a unique pH profile. The SQ_{Nf} EPR signals were readily detectable only between pH 7.0 and pH 8.5, and the signal amplitudes were roughly constant. The signal amplitudes paralleled the NADH−Q_1 oxidoreductase activity in the absence of CCCP. The SQ_{Nf} species was only kinetically trapped in the $\Delta\mu_{H^+}$ posed steady-state thus far. We did not detect any SQ species equivalent to the SQ_{Nf} in SMP in the absence of $\Delta\mu_{H^+}$ by a redox titration method (Yano et al., unpublished data). The electron transfer from NADH to cluster N2 does not limit turnover of the enzyme. The $\Delta\mu_{H^+}$ slows down the electron-transfer process from cluster N2 to the Q-pool whereby the $[(N2)_{red}-SQ_{Nf}]$ becomes readily detectable. This part of the electron-transfer pathway is highly sensitive to $\Delta\mu_{H^+}$; therefore, the SQ_{Nf} species can be seen even with 1.2−1.5 of RCR as described in the present study. This unambiguously confirms that this SQ_{Nf} species is involved in the energy coupling reactions (*34*, *35*, *38*).

The PSST subunit is an essential subunit of the catalytic core unit along with 49 kDa, TYKY, 30 kDa, ND1, and H^+ transport pathway forming subunits (ND2/4/5). The location of cluster N2 in the PSST has been confirmed by the recent site-directed mutagenesis and EPR characterization of *E. coli* complex I (*20*, *57*). The site-directed mutagenesis of the PSST and 49 kDa subunit homologues of *Y. lipolytica* complex I have provided evidence that cluster N2 is locatedin the PSST close to the interface to the 49 kDa subunit (*58*, *59*). PSST, 49 kDa, ND1, and ND5 subunits are also known to be specific binding sites of potent complex I inhibitors (*27*, *29*, *60*−*63*). The catalytic unit of complex I is structurally highly homologous to the energy-transducing membrane-bound [NiFe] hydrogenases (e.g., *Methanosarcina barkeri* Ech), indicating that they are evolutionarily closely related (*64*−*69*). The PSST subunit is homologous to the binding domain of the $[4Fe-4S]_{proximal}$ cluster of the subunit (e.g., EchC) of the [NiFe] hydrogenases; however, the cluster binding motif for cluster N2 in the PSST subunit (**CC**...GxCxxxG...PGC) is different from that for the $[4Fe-4S]_{proximal}$ cluster (**CxxC**...GxCxxxG...PGC) in the hydrogenase subunit. Only three cysteine residues are in common between complex I and [NiFe] hydrogenases. It has been suggested that either the fourth ligand is a noncysteinyl residue of the PSST subunit or is provided from a neighboring subunit (49 kDa subunit) (*22*, *66*, *70*) or that the two adjacent cysteines may be able to coordinate to a single [4Fe−4S] cluster by overcoming steric hindrance (*20*). The latter possibility has recently been examined by a means of the molecular dynamic calculation using the X-ray structure of the small subunit of the *Desulfovibrio gigas* hydrogenase that houses the $[4Fe-4S]_{proximal}$ cluster, suggesting that such a coordination can be allowed (*71*). Although this important issue remains to be addressed in the future, it is certain that the ligand coordination of cluster N2 is exceptional; therefore, it is proposed that the PSST subunit and its neighboring subunits contain specific structures to aid electron transfer from cluster N2 to Q. It has been proposed that such significant changes in the iron−sulfur cluster binding sequence motif occurred in the PSST subunit as well as some sequence changes in the 49 kDa and ND1 subunits are associated with the changes in its physiological functions from "hydrogenase" to "Q-reductase" during the evolution of complex I (*72*). In this connection, the unique $[(N2)_{red}-SQ_{Nf}]$ transition intermediate state captured in this study is one proof that complex I has evolutionarily acquired the ability to facilitate rapid energy-coupled electron transfer to Q by modifying the local structures in the catalytic core unit subunits (*72*). It is suggested that the exchange coupled $[(N2)_{red}-SQ_{Nf}]$ species constitutes an integrated part of the energy-coupling machinery in the catalytic core unit. It is hypothesized that the formation of the $[(N2)_{red}-SQ_{Nf}]$ species is a prerequisite to convert the redox energy to the electrochemical potential energy. The formation of the $[(N2)_{red}-SQ_{Nf}]$ species may trigger charge or structural arrangements or both in and around this vicinity as an essential step of the gating system for the H^+ pump in the membrane part of complex I. One such arrangement can be provided by nearby carboxylates the p*K*'s of which change in response to the change in the redox states of cluster N2 and/or SQ_{Nf}. Local motions of such amino acid residues may promote H^+

transfer (*73*, *74*). Potential amino acid residues, for example, aspartic acid, glutamic acid, or tyrosine are conserved in the catalytic core subunits, PSST and 49 kDa subunits, and the involvement of carboxylates responding to the redox reactions have been reported (*22*, *75*, *76*). Such local rearrangements may induce rather large conformational changes.

In summary, the present study has provided the first direct evidence of the mutual interaction between cluster N2 and the $\Delta\mu_{H^+}$-sensitive SQ_{Nf} by a means of the spin−spin interaction. The characterizations of the exchange-coupled $[(N2)_{red}-SQ_{Nf}]$ species have revealed that this intermediate redox species is involved in the electron-transfer processes that are tightly coupled to the $\Delta\mu_{H^+}$ formation.

ACKNOWLEDGMENT

Authors would like to express their gratitude to Dr. John Salerno for his stimulating comments and discussions.

REFERENCES

1. Weiss, H., Friedrich, T., Hofhaus, G., and Preis, D. (1991) The respiratory-chain NADH dehydrogenase (complex I) of mitochondria, *Eur. J. Biochem. 197*, 563−576.
2. Walker, J. E. (1992) The NADH:ubiquinone oxidoreductase (complex I) of respiratory chains, *Q. Rev. Biophys. 25*, 253−324.
3. Ohnishi, T. (1998) Iron−sulfur clusters/semiquinones in complex I, *Biochim. Biophys. Acta 1364*, 186−206.
4. Yano, T. (2002) The energy-transducing NADH: quinone oxidoreductase, complex I, *Mol. Aspects Med. 23*, 345−368.
5. Hirst, J., Carroll, J., Fearnley, I. M., Shannon, R. J., and Walker, J. E. (2003) The nuclear encoded subunits of complex I from bovine heart mitochondria, *Biochim. Biophys. Acta 1604*, 135−150.
6. Guènebaut, V., Vincentelli, R., Mills, D., Weiss, H., and Leonard, K. R. (1997) Three-dimensional structure of NADH-dehydrogenase from *Neurospora crassa* by electron microscopy and conical tilt reconstruction, *J. Mol. Biol. 265*, 409−418.
7. Guènebaut, V., Schlitt, A., Weiss, H., Leonard, K. R., and Friedrich, T. (1998) Consistent structure between bacterial and mitochondrial NADH: ubiquinone oxidoreductase (complex I), *J. Mol. Biol. 276*, 105−112.
8. Grigorieff, N. (1998) Three-dimensional structure of bovine NADH:ubiquinone oxidoreductase (complex I) at 22 Å in ice, *J. Mol. Biol. 277*, 1033−1046.
9. Grigorieff, N. (1999) Structure of the respiratory NADH:ubiquinone oxidoreductase (complex I), *Curr. Opin. Struct. Biol. 9*, 476−483.
10. Djafarzadeh, R., Kerscher, S., Zwicker, K., Radermacher, M., Lindahl, M., Schägger, H., and Brandt, U. (2000) Biophysical and structural characterization of proton-translocating NADH-dehydrogenase (complex I) from the strictly aerobic yeast *Yarrowia lipolytica*, *Biochim. Biophys. Acta 1459*, 230−238.
11. Böttcher, B., Scheide, D., Hesterberg, M., Nagel-Steger, L., and Friedrich, T. (2002) A novel, enzymatically active conformation of the *Escherichia coli* NADH: ubiquinone oxidoreductase (complex I), *J. Biol. Chem. 277*, 17970−17977.
12. Hatefi, Y. (1985) The mitochondrial electron transport and oxidative phosphorylation system, *Annu. Rev. Biochem. 54*, 1015−1069.
13. Yano, T., Magnitsky, S., Sled′, V. D., Ohnishi, T., and Yagi, T. (1999) Characterization of the putative 2x[4Fe-4S] binding NQO9 subunit of the proton translocating NADH-quinone oxidoreductase (NDH-1) of *Paracoccus denitrificans*: Expression, reconstitution, and EPR characterization, *J. Biol. Chem. 274*, 28598−28605.
14. Rasmussen, T., Scheide, D., Brors, B., Kintscher, L., Weiss, H., and Friedrich, T. (2001) Identification of two tetranuclear FeS clusters on the ferredoxin-type subunit of NADH:ubiquinone oxidoreductase (complex I), *Biochemistry 40*, 6124−6131.
15. Yano, T., Sled′, V. D., Ohnishi, T., and Yagi, T. (1994) Expression of the 25-kilodalton iron−sulfur subunit of the energy-transducing NADH-ubiquinone oxidoreductase of *Paracoccus denitrificans*, *Biochemistry 33*, 494−499.
16. Leif, H., Sled′, V. D., Ohnishi, T., Weiss, H., and Friedrich, T. (1995) Isolation and characterization of the proton-translocating NADH:ubiquinone oxidoreductase from *Escherichia coli*, *Eur. J. Biochem. 230*, 538−548.
17. Yano, T., Yagi, T., Sled′, V. D., and Ohnishi, T. (1995) Expression and characterization of the 66-Kilodalton (NQO3) iron−sulfur subunit of the proton-translocating NADH-quinone oxidoreductase of *Paracoccus denitrificans*, *J. Biol. Chem. 270*, 18264−18270.
18. Yano, T., Sled′, V. D., Ohnishi, T., and Yagi, T. (1996) Expression and characterization of the flavoprotein subcomplex composed of 50-kDa (NQO1) and 25-kDa (NQO2) subunits of the proton-translocating NADH-quinone oxidoreductase of *Paracoccus denitrificans*, *J. Biol. Chem. 271*, 5907−5913.
19. Yano, T., Sklar, J., Nakamaru-Ogiso, E., Takahashi, Y., Yagi, T., and Ohnishi, T. (2003) Characterization of cluster N5 as a fast-relaxing [4Fe-4S] cluster in the Nqo3 subunit of the proton-translocating NADH-ubiquinone oxidoreductase from *Paracoccus denitrificans*, *J. Biol. Chem. 278*, 15514−15522.
20. Flemming, D., Schlitt, A., Spehr, V., Bischof, T., and Friedrich, T. (2003) Iron−sulfur cluster N2 of the *Escherichia coli* NADH: ubiquinone oxidoreductase (complex I) is located on subunit NuoB, *J. Biol. Chem. 278*, 47602−47609.
21. Ingledew, W. J., and Ohnishi, T. (1980) An analysis of some thermodynamic properties of iron−sulfur centres in site I of mitochondria, *Biochem. J. 186*, 111−117.
22. Garofano, A., Zwicker, K., Kerscher, S., Okun, P., and Brandt, U. (2003) Two aspartic acid residues in the PSST-homologous NUKM subunit of complex I from *Yarrowia lipolytica* are essential for catalytic activity, *J. Biol. Chem. 278*, 42435−42440.
23. Hamamoto, T., Hashimoto, M., Hino, M., Kitada, M., Seto, Y., Kudo, T., and Horikoshi, K. (1994) Characterization of a gene responsible for the Na^+/H^+ antiporter system of alkalophilic *Bacillus* species strain C-125, *Mol. Microbiol. 14*, 939−946.
24. Hiramatsu, T., Kodama, K., Kuroda, T., Mizushima, T., and Tsuchiya, T. (1998) A putative multisubunit Na^+/H^+ antiporter from *Staphylococcus aureus*, *J. Bacteriol. 180*, 6642−6648.
25. Ito, M., Guffanti, A. A., and Krulwich, T. A. (2001) Mrp-dependent Na^+/H^+ antiporters of *Bacillus* exhibit characteristics that are unanticipated for completely secondary active transporters, *FEBS Lett. 496*, 117−120.
26. Zickermann, V., Barquera, B., Wikstrom, M., and Finel, M. (1998) Analysis of the pathogenic human mitochondrial mutation ND1/3460, and mutations of strictly conserved residues in its vicinity, using the bacterium *Paracoccus denitrificans*, *Biochemistry 37*, 11792−11796.
27. Schuler, F., Yano, T., Di Bernardo, S., Yagi, T., Yankovskaya, V., Singer, P. T., and Casida, J. E. (1999) NADH-quinone oxidoreductase: PSST subunit couples electron transfer from iron−sulfur cluster N2 to quinone, *Proc. Natl. Acad. Sci. U.S.A. 96*, 4149−4153.
28. Schuler, F., and Casida, J. E. (2001) Functional coupling of PSST and ND1 subunits in NADH:ubiquinone oxidoreductase established by photoaffinity labeling, *Biochim. Biophys. Acta 1506*, 79−87.
29. Nakamaru-Ogiso, E., Sakamoto, K., Matsuno-Yagi, A., Miyoshi, H., and Yagi, T. (2003) The ND5 subunit was labeled by a photoaffinity analogue of fenpyroximate in bovine mitochondrial complex I, *Biochemistry 42*, 746−754.
30. Nakamaru-Ogiso, E., Seo, B. B., Yagi, T., and Matsuno-Yagi, A. (2003) Amiloride inhibition of the proton-translocating NADH-quinone oxidoreductase of mammals and bacteria, *FEBS Lett. 549*, 43−46.
31. Amarneh, B., and Vik, S. B. (2003) Mutagenesis of subunit N of the *Escherichia coli* complex I. Identification of the initiation codon and the sensitivity of mutants to decylubiquinone, *Biochemistry 42*, 4800−4808.
32. Gong, X., Xie, T., Yu, L., Hesterberg, M., Scheide, D., Friedrich, T., and Yu, C. A. (2003) The ubiquinone-binding site in NADH: ubiquinone oxidoreductase from *Escherichia coli*, *J. Biol. Chem. 278*, 25731−25737.
33. Fisher, N., and Rich, P. R. (2000) A motif for quinone binding sites in respiratory and photosynthetic systems, *J. Mol. Biol. 296*, 1153−1162.
34. Magnitsky, S., Toulokhonova, L., Yano, T., Sled, V. D., Hägerhäll, C., Grivennikova, V. G., Burbaev, D. S., Vinogradov, A. D., and Ohnishi, T. (2002) EPR characterization of ubisemiquinones and iron−sulfur cluster N2, central components of the energy coupling in the NADH-ubiquinone oxidoreductase (complex I) in situ, *J. Bioenerg. Biomembr. 34*, 193−208.
35. Vinogradov, A. D., Sled′, V. D., Burbaev, D. S., Grivennikova, V. G., Moroz, I. A., and Ohnishi, T. (1995) Energy-dependent

complex I-associated u bisemiquinones in submitochondrial particles, *FEBS Lett. 370*, 83−87.
36. Burbaev, D. S., Moroz, I. A., Kotlyar, A. B., Sled, V. D., and Vinogradov, A. D. (1989) Ubisemiquinone in the NADH-ubiquinone reductase region of the mitochondrial respiratory chain, *FEBS Lett. 254*, 47−51.
37. Ohnishi, T., Sled′, V. D., Yano, T., Yagi, T., Burbaev, D. S., and Vinogradov, A. D. (1998) Structure−function studies of iron−sulfur clusters and semiquinones in the NADH-Q oxidoreductase segment of the respiratory chain, *Biochim. Biophys. Acta 1365*, 301−308.
38. Yano, T., Magnitsky, S., and Ohnishi, T. (2000) Characterization of the complex I-associated ubisemiquinone species: toward the understanding of their functional roles in the electron/proton-transfer reaction, *Biochim. Biophys. Acta 1459*, 299−304.
39. Dunham, W. R., Hagen, W. R., Fee, J. A., Sands, R. H., Dunbar, J. B., and Humblet, C. (1991) An investigation of *Chromatium vinosum* high-potential iron−sulfur protein by EPR and Mossbauer spectroscopy; evidence for a freezing-induced dimerization in NaCl solutions, *Biochim. Biophys. Acta 1079*, 253−262.
40. Stevenson, R. C., Dunham, W. R., Sands, R. H., Singer, T. P., and Beinert, H. (1986) Studies on the spin−spin interaction between flavin and iron−sulfur cluster in an iron−sulfur flavoprotein, *Biochim. Biophys. Acta 869*, 81−88.
41. Kotlyar, A. B., and Vinogradov, A. D. (1990) Slow active/inactive transition of the mitochondrial NADH-ubiquinone reductase, *Biochim. Biophys. Acta 1019*, 151−158 [published erratum appears in (1990) *Biochim. Biophys. Acta 1020* (1), 113].
42. Grivennikova, V. G., Maklashina, E. O., Gavrikova, E. V., and Vinogradov, A. D. (1997) Interaction of the mitochondrial NADH-ubiquinone reductase with rotenone as related to the enzyme active/inactive transition, *Biochim. Biophys. Acta 1319*, 223−232.
43. Schepler, K. L., Dunham, W. R., Sands, R. H., Fee, J. A., and Abeles, R. H. (1975) A physical explanation of the EPR spectrum observed during catalysis by enzymes utilizing coenzyme B12, *Biochim. Biophys. Acta 397*, 510−518.
44. Ruzicka, F. J., Beinert, H., Schepler, K. L., Dunham, W. R., and Sands, R. H. (1975) Interaction of ubisemiquinone with a paramagnetic component in heart tissue, *Proc. Natl. Acad. Sci. U.S.A. 72*, 2886−2890.
45. Hagen, W. R., Hearshen, D. O., Sands, R. H., and Dunham, W. R. (1985) A statistical theory for powder EPR in distributed systems, *J. Magn. Reson. 61*, 220−232.
46. Hagen, W. R., Hearshen, D. O., Harding, L. J., and Dunham, W. R. (1985) Quantitative numerical analysis of g strain in the EPR of distributed systems; its importance for multicenter metalloproteins, *J. Magn. Reson. 61*, 233−244.
47. Hearshen, D. O., Hagen, W. R., Sands, R. H., Grande, H. J., and Dunham, W. R. (1986) An analysis of g-strain in the EPR of two [2Fe−2S] ferredoxins. Evidence for a protein rigidity model, *J. Magn. Reson. 69*, 440−469.
48. Dunham, W. R., Fee, J. A., Harding, L. J., and Grande, H. J. (1980) Application of fast Fourier transformations to EPR spectra of free radicals in solution, *J. Magn. Reson. 40*, 351−359.
49. Abragam, A., and Bleaney, B. (1970) *Electron paramagnetic resonance of transition ions*, Calendar Press, Oxford, U.K.
50. van Belzen, R., Kotlyar, A. B., Moon, N., Dunham, W. R., and Albracht, S. P. J. (1997) The iron−sulfur clusters 2 and ubisemiquinone radicals of NADH:ubiquinone oxidoreductase are involved in energy coupling in submitochondrial particles, *Biochemistry 36*, 886−893.
51. Degli Esposti, M., Ngo, A., McMullen, G. L., Ghelli, A., Sparla, F., Benelli, B., Ratta, M., and Linnane, A. W. (1996) The specificity of mitochondrial complex I for ubiquinones, *Biochem. J. 313*, 327−334.
52. Salerno, J. C., Blum, H., and Ohnishi, T. (1979) The orientation of iron−sulfur clusters and a spin-coupled ubiquinone pair in the mitochondrial membrane, *Biochim. Biophys. Acta 547*, 270−281.
53. Ohnishi, T., Magnitsky, S., Toulokhonova, T., Yano, T., Yagi, T., Burbaev, D. S., Vinogradov, A., and Sled′, V. D. (1999) EPR studies of the possible binding sites of the cluster N2, semiquinone, and specific inhibitors of the NADH:quinone oxidoreductase (complex I), *Biochem. Soc. Trans. 27*, 586−591.
54. Salerno, J. C., and Ohnishi, T. (1980) Studies on the stabilized ubisemiquinone species in the succinate-cytochrome *c* reductase segment of the intact mitochondrial membrane system, *Biochem. J. 192*, 769−781.
55. Meinhardt, S. W., Yang, X., Trumpower, B. L., and Ohnishi, T. (1987) Identification of a stable ubisemiquinone and characterization of the effects of ubiquinone oxidation−reduction status on the Rieske iron−sulfur protein in the three-subunit ubiquinol-cytochrome *c* oxidoreductase complex of *Paracoccus denitrificans*, *J. Biol. Chem. 262*, 8702−8706.
56. Okamura, M. Y., Paddock, M. L., Graige, M. S., and Feher, G. (2000) Proton and electron transfer in bacterial reaction centers, *Biochim. Biophys. Acta 1458*, 148−163.
57. Duarte, M., Populo, H., Videira, A., Friedrich, T., and Schulte, U. (2002) Disruption of iron-sulphur cluster N2 from NADH: ubiquinone oxidoreductase by site-directed mutagenesis, *Biochem. J. 364*, 833−839.
58. Ahlers, P. M., Zwicker, K., Kerscher, S., and Brandt, U. (2000) Function of conserved acidic residues in the PSST homologue of complex I (NADH:ubiquinone oxidoreductase) from *Yarrowia lipolytica*, *J. Biol. Chem. 275*, 23577−23582.
59. Grgic, L., Zwicker, K., Kashani-Poor, N., Kerscher, S., and Brandt, U. (2004) Functional significance of conserved histidines and arginines in the 49-kDa subunit of mitochondrial complex I, *J. Biol. Chem. 279*, 21193-21199.
60. Darrouzet, E., and Dupuis, A. (1997) Genetic evidence for the existence of two quinone related inhibitor binding sites in NADH−CoQ reductase, *Biochim. Biophys. Acta 1319*, 1−4.
61. Prieur, I., Lunardi, J., and Dupuis, A. (2001) Evidence for a quinone binding site close to the interface between NUOD and NUOB subunits of Complex I, *Biochim. Biophys. Acta 1504*, 173−178.
62. Earley, F. G., Patel, S. D., Ragan, C. I., and Attardi, G. (1987) Photolabeling of a mitochondrially encoded subunit of NADH dehydrogenase with [3-H]-dehydrorotenone, *FEBS Lett. 219*, 108−113.
63. Earley, F. G., and Ragan, C. I. (1984) Photoaffinity labeling of mitochondrial NADH dehydrogenase with arylazidoamorphigenin, an analogue of rotenone, *Biochem. J. 224*, 525−534.
64. Kunkel, A., Vorholt, J. A., Thauer, R. K., and Hedderich, R. (1998) An *Escherichia coli* hydrogenase-3-type hydrogenase in methanogenic archaea, *Eur. J. Biochem. 252*, 467−476.
65. Meuer, J., Bartoschek, S., Koch, J., Kunkel, A., and Hedderich, R. (1999) Purification and catalytic properties of Ech hydrogenase from *Methanosarcina barkeri*, *Eur. J. Biochem. 265*, 325−335.
66. Kashani-Poor, N., Zwicker, K., Kerscher, S., and Brandt, U. (2001) A central functional role for the 49-kDa subunit within the catalytic core of mitochondrial complex I, *J. Biol. Chem. 276*, 24082−24087.
67. Friedrich, T., and Weiss, H. (1997) Modular evolution of the respiratory NADH:ubiquinone oxidoreductase and the origin of its modules, *J. Theor. Biol. 187*, 529−540.
68. Friedrich, T., and Scheide, D. (2000) The respiratory complex I of bacteria, archaea and eukarya and its module common with membrane-bound multisubunit hydrogenases, *FEBS Lett. 479*, 1−5.
69. Hedderich, R. (2004) Energy-converting [NiFe] hydrogenases from archaea and extremophiles: ancestors of complex I, *J. Bioenerg. Biomembr. 36*, 65−75.
70. Brandt, U., Kerscher, S., Drose, S., Zwicker, K., and Zickermann, V. (2003) Proton pumping by NADH:ubiquinone oxidoreductase. A redox driven conformational change mechanism? *FEBS Lett. 545*, 9−17.
71. Gurrath, M., and Friedrich, T. (2004) Adjacent cysteines are capable of ligating the same tetranuclear iron−sulfur cluster, *Proteins 56*, 556−563.
72. Yano, T., and Ohnishi, T. (2001) The origin of cluster N2 of the energy-transducing NADH-quinone oxidoreductase: comparisons of phylogenetically related enzymes, *J. Bioenerg. Biomembr. 33*, 213−222.
73. Camba, R., Jung, Y. S., Hunsicker-Wang, L. M., Burgess, B. K., Stout, C. D., Hirst, J., and Armstrong, F. A. (2003) Mechanisms of redox-coupled proton transfer in proteins: role of the proximal proline in reactions of the [3Fe-4S] cluster in *Azotobacter vinelandii* ferredoxin I, *Biochemistry 42*, 10589−10599.
74. Chen, K., Hirst, J., Camba, R., Bonagura, C. A., Stout, C. D., Burgess, B. K., and Armstrong, F. A. (2000) Atomically defined mechanism for proton transfer to a buried redox centre in a protein, *Nature 405*, 814−817.

75. Flemming, D., Hellwig, P., and Friedrich, T. (2003) Involvement of tyrosines 114 and 139 of subunit NuoB in the proton pathway around cluster N2 in *Escherichia coli* NADH:ubiquinone oxidoreductase, *J. Biol. Chem. 278*, 3055−3062.
76. Hellwig, P., Scheide, D., Bungert, S., Mantele, W., and Friedrich, T. (2000) FT-IR spectroscopic characterization of NADH:ubiquinone oxidoreductase (complex I) from *Escherichia coli*: oxidation of FeS cluster N2 is coupled with the protonation of an aspartate or glutamate side chain, *Biochemistry 39*, 10884−10891.
77. Ohnishi, T., Johnson, Jr., J. E., Yano, T., LaBrutto, R., Widger, W. R., FEBS Lett., in press.

BI048132I